ORIGINAL ARTICLE

ALD-induced TiO$_2$/Ag nanofilm for rapid surface photodynamic ion sterilization

Peng-Fei Cai, Jun Li, Xin-Bao Wu*, Zhao-Yang Li, Jie Shen*, Jing-Jun Nie, Zhen-Duo Cui, Da-Fu Chen*, Yan-Qin Liang, Sheng-Li Zhu, Shui-Lin Wu*

Abstract The daily life of people in the intelligent age is inseparable from electronic device, and a number of bacteria on touch screens are increasingly threatening the health of users. Herein, a photocatalytic TiO$_2$/Ag thin film was synthesized on a glass by atomic layer deposition and subsequent in situ reduction. Ultraviolet–visible (UV-Vis) spectra showed that this film can harvest the simulated solar light more efficiently than that of pristine TiO$_2$. The antibacterial tests in vitro showed that the antibacterial efficiency of the TiO$_2$/Ag film against *S. aureus* and *E. coli* was 98.2% and 98.6%, under visible light irradiation for 5 min. The underlying mechanism was that the in-situ reduction of Ag on the surface of TiO$_2$ reduced the bandgap of TiO$_2$ from 3.44 to 2.61 eV due to the formation of Schottky heterojunction at the interface between TiO$_2$ and Ag. Thus, TiO$_2$/Ag can generate more reactive oxygen species for bacterial inactivation on the surface of electronic screens. More importantly, the TiO$_2$/Ag film had great biocompatibility with/without light irradiation. The platform not only provides a more convenient choice for the traditional antibacterial mode but also has limitless possibilities for application in the field of billions of touch screens.

Keywords Antibacterial; Photoresponsive; Photodynamic; Surface sterilization; Atomic layer deposition (ALD)

P.-F. Cai, J. Li, Z.-Y. Li, Z.-D. Cui, Y.-Q. Liang, S.-L. Zhu, S.-L. Wu*
School of Materials Science & Engineering, The Key Laboratory of Advanced Ceramics and Machining Technology by the Ministry of Education of China, Tianjin University, Tianjin 300072, China
e-mail: shuilinwu@tju.edu.cn

X.-B. Wu*
Department of Orthopedic Trauma, Beijing Jishuitan Hospital, Beijing 100035, China
e-mail: wuxinbao_jst@126.com

J. Shen*
Shenzhen Key Laboratory of Spine Surgery, Department of Spine Surgery, Peking University Shenzhen Hospital, Shenzhen 518041, China
e-mail: jayjayson909@gmail.com

J.-J. Nie, D.-F. Chen*
Laboratory of Bone Tissue Engineering, Beijing Laboratory of Biomedical Materials, Beijing Research Institute of Orthopaedics and Traumatology, Beijing Jishuitan Hospital, Beijing 100035, China
e-mail: chendafujst@126.com

1 Introduction

Since the spread of coronavirus pandemic in 2019, healthy life has attracted more people's attention, especially the demand for effective antibacterial materials [1]. At the same time, with the advent of the intelligent society and the popularization of electronic products, billions of touch screens have been popularized in people's lives. However, the species and quantities of bacteria on the surface of them are affecting people's health [2, 3]. At present, traditional antibacterial methods include antibiotics, inorganic antibacterial agents (such as Cu, Ag, Au) [4–6], and organic antibacterial agents (quaternary ammonium salts, etc.) [7]. Since the discovery of penicillin by Alexander Fleming in the early twentieth century, antibiotics have been widely utilized to treat diseases caused by bacterial infections. However, the overuse and abuse of antibiotics have led to the emergence of bacterial resistance, even the birth of "super bacteria" [8]. Metal ions on the carrier

through physical or chemical means can kill the microbes by destroying the cell membrane, which has strong bactericidal ability, low toxicity, and high safety. However, the expensive cost and unpromising durability limit its application [9]. Further, organic antibacterial agents have fast sterilization speed and high stability, but they are prone to the development of drug resistance, and the decomposition products are toxic to human body [10].

In the post-antibiotic era, photocatalytic sterilization is an effective antibacterial method. Photoactivated sterilization refers to the use of light with appropriate wavelengths, ranging from ultraviolet (UV) to near-infrared (NIR), to activate photoresponsive materials [11–16]. Photoresponsive materials can absorb light energy to effectively kill pathogens in a short time through the synergy of heat and reactive oxygen species (ROS) such as O_2^-, ·OH, $^1O_2$, generated by photocatalysts [17–22]. Among various semiconductor-based photocatalysts, TiO$_2$ has appeared as the leading candidate due to its high photoactivity, superior chemical stability, and broad-spectrum antibacterial property. However, the higher energy band gap limits the application of TiO$_2$ under visible light [23]. At the same time, the low rate of electron transfer to oxygen and the high electron–hole recombination rate of TiO$_2$ also inhibit the production of ROS [24]. Therefore, many efforts have been devoted to improving visible light absorbance by modifying TiO$_2$ nanoparticles (NPs), including element doping, heterojunction structure, noble metal deposition, and so on [25–30].

Among the commonly used preparation methods of TiO$_2$ coating, atomic layer deposition (ALD) has great advantages such as accurate thickness control, outstanding atomic-scale uniformity, and saturated surface reactions compared with other deposition methods [31–34]. Further, as one of the effective methods, noble metals can act as electron traps which are close to conduction bands of semiconductors or improve the excitation of surface electrons through surface plasmon resonance effects, thereby reducing the recombination of photoinduced carriers in noble metal/semiconductor [35–37]. On the other hand, the cell membranes of microorganisms are mostly negatively charged, while metal ions are positively charged, so they can firmly adhere to the cell membrane by electrostatic interaction and further penetrate the cell wall into the bacterial cell membrane [38]. Thus, TiO$_2$ deposited silver or other noble metals, which can not only effectively prevent recombination of electron–hole pairs, but also enhance the photocatalytic effect of TiO$_2$ under visible light, thereby enhancing the antibacterial efficiency of composite materials [39, 40].

In this work, we prepared a TiO$_2$ nanofilm by ALD, then Ag particles were deposited on the surface by photo-reduction. Due to the different Fermi levels of TiO$_2$ and Ag, they can form Schottky barrier which can efficiently improve the separation of electrons and holes. Therefore, more ROS can be generated under visible light. The platform showed great antibacterial efficiency against *Staphylococcus aureus* (*S. aureus,* 98.2%) and *Escherichia coli* (*E. coli*, 98.6%) under the conditions of simulated sunlight for 5 min, respectively. The excellent antimicrobial effects of TiO$_2$/Ag nanofilm under visible light illumination open up new possibilities, such as continuous visible light-powered disinfection during daytime and at night, for a broad range of surface disinfection application.

2 Experimental

2.1 Preparation of TiO$_2$ nanofilms

Firstly, glass slides (2 cm × 2 cm) were ultrasonically cleaned with acetone, ethanol, and distilled water for 30 min to remove stains on their surface. Then TiO$_2$ nanofilm was deposited on glass slides by plasma-enhanced ALD (MNT-P-100–43, Micro and Nanotech Co, LTD, Wuxi, China). Tetrakis(diethylamino)titanium (TDMAT) as titanium precursor and H$_2$O as oxygen precursor were kept at 75 °C and 25 °C, respectively. The reaction temperature was 200 °C and the base pressure was 25 Pa with high purity N$_2$ during deposition. Each cycle consisted of precursor exposure and N$_2$ purging following a sequence of H$_2$O:N$_2$:TDEAT:N$_2$ with a corresponding duration of 0.1:15:0.1:20 s. The reaction was repeated for 200 cycles to produce TiO$_2$ nanofilms.

2.2 Synthesis of TiO$_2$/Ag nanofilms

Silver nitrate aqueous solution (0.05 mol·L^{-1}, 400 μl) was dropped onto surface of TiO$_2$ nanofilm, then it was placed in a 60 °C oven. To spread the silver ions uniformly on the surface of TiO$_2$, a xenon lamp was used to irradiate it for 50 min. The ultraviolet light could quickly reduce the silver ions into silver nanoparticles, with the color of the surface changed from transparent to light gray. The Ag nanofilm was also fabricated in the same way.

2.3 Morphological and structural characterization

The morphology of TiO$_2$ and TiO$_2$/Ag was observed by scanning electron microscopy (SEM, S-4800, Hitachi, Japan). Water contact angle (JC2000D Contact Angle system, POWER EACH) measurement was conducted to analyze the hydrophilic property of surfaces of TiO$_2$ and TiO$_2$/Ag. The surface elemental composition of the samples was obtained using X-ray photoelectron spectroscopy (XPS, ESCALAB 250Xi). Ultraviolet–visible–NIR (UV–

Vis–NIR) spectrometer (UV-2700, Shimadzu, Japan) was used to obtain samples' optical properties.

2.4 Photoelectrochemical measurement

A three-electrode system in quartz glass cell in $0.5 \text{ mol} \cdot \text{L}^{-1}$ Na_2SO_4 aqueous solution was performed to measure the photocurrent response. Pt plate as counter electrode, an Ag/AgCl electrode as reference electrode, and an experimental sample as working electrode was used to analyze electrochemical impedance spectroscopy (EIS). The photoinduced current densities of the photocurrent response with time (*i-t* curve) were measured at a 0 V bias potential under xenon lamp (PLS-SXE300, Beijing Changming Technology Co., Ltd, China) irradiation. EIS tests were recorded over the frequency range from 1×10^4 to 1×10^{-1} Hz with an alternating current voltage magnitude of 5 mV under simulated visible light irradiation. The experimental samples (TiO_2 and TiO_2/Ag) were prepared on ITO conductive glasses (2 cm × 2 cm).

2.5 Detection of ROS

Electron spin resonance (ESR) spectra were recorded on a JES-FA200 spectrometer. 5,5-dimethyl-1-pyrroline-N-oxide (DMPO) (Sigma) was used to trap ·OH and $·O_2^-$ under xenon lamp irradiation. The glass slides, TiO_2' and TiO_2/Ag samples were immersed in $100 \text{ mmol} \cdot \text{L}^{-1}$ DMPO at ambient temperature under xenon lamp irradiation (PLS-SXE300/300UV).

2.6 Evaluation of antibacterial activity

The spread plate method was used to study the antibacterial activity of the samples (including pure glass slide, TiO_2, Ag, and TiO_2/Ag) under stimulated visible light irradiation. *E. coli* (Gram-negative, ATCC 25,922) and *S. aureus* (Gram-positive, ATCC 29,213) were used for antibacterial experiments. All bacteria were cultured in Luria–Bertani (LB) medium. The pure glass slide was set as the control group and TiO_2, Ag and TiO_2/Ag constituted the experimental groups. The details were as follows: 40 µl of bacterial suspension ($\sim 1 \times 10^4 \text{ CFU} \cdot \text{ml}^{-1}$) was dropped onto the surface of the samples (2 mm × 2 mm glass slide). After 5 min with or without stimulated visible light irradiation, the samples were put upside down on the LB agar plates, then incubated at 37 °C for 1 h. Next, the glass slide was removed from the LB plates, and the LB plates were still incubated at 37 °C for 24 h for bacterial counts. Three parallel samples from each group were used in the antibacterial test. The antibacterial efficiency of each sample was calculated by the number of bacterial colonies on the glass slide using Eq. (1):

$$\text{Antibacterial ratio} = \frac{\text{CFU}_{\text{Control}} - \text{CFU}_{\text{Sample}}}{\text{CFU}_{\text{Control}}} \times 100\% \quad (1)$$

where $\text{CFU}_{\text{control}}$ indicates the growth of bacteria without treatment and $\text{CFU}_{\text{sample}}$ indicates the growth of bacteria with sample cotreatment.

To better analyze the bacterial morphologies, the bacterial morphology study was evaluated using SEM. After 5 min stimulated visible light irradiation, the *E. coli* and *S. aureus* on the samples were fixed with a 2.5 wt% glutaraldehyde solution for 2 h, then washed with phosphate buffer saline (PBS, pH = 7.0). Further, the bacteria were dehydrated using graded ethanol solutions (20, 40, 60, 80, and 100 wt%) for 15 min. After drying, the morphologies and microstructures were observed by SEM.

2.7 Cytotoxicity assay

L929 fibroblast cells were cultured in Roswell Park Memorial Institute 1640 (RPMI 1640, Meilunbio) including 10% (*v/v*) fetal bovine serum and 1 wt% penicillin–streptomycin. The cells were placed in an incubator at 37 °C with 95% humidity and 5% CO_2. The cell culture medium was replaced regularly every other day. To investigate the cytotoxicity of TiO_2, Ag, and TiO_2/Ag, the sterilized samples (Φ8 mm) were put into 48-well plates, and 400 µl L929 ($1 \times 10^5 \text{ cells} \cdot \text{ml}^{-1}$) were added to the plates. Then each type of sample was treated with or without light irradiation. The cells were cultured in samples for 24 h under the same conditions. After that, the culture medium was removed and 200 µl $0.05 \text{ mg} \cdot \text{ml}^{-1}$ MTT (dissolved MTT powder into pH 7.4 PBS solution) solution was added to each well. Next, the culture medium was incubated for 4 h at 37 °C in an atmosphere of 5% CO_2 and 95% air until purple precipitate appeared. Then, MTT solution was removed, then 200 µl of dimethyl sulfoxide (DMSO) was added to each well with continuous shaking for 15 min to dissolve the purple precipitate. Finally, the samples were taken out, and the optical density (OD) of liquid was tested at 490 nm with a microplate reader. The cell viability was calculated using Eq. (2):

$$\text{Cell viability} = \frac{\text{OD in experiment group}}{\text{OD in control group}} \times 100\% \quad (2)$$
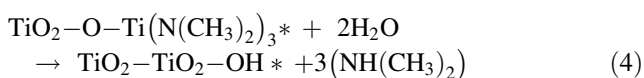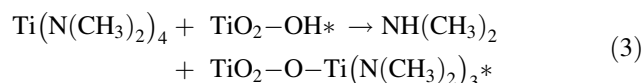
2.8 Statistical analysis

All the quantitative data were analyzed by one-way analysis of variance (ANOVA) and expressed as mean values ± standard deviations with $n = 3$ (3 biologically independent samples). A student t-test was performed to evaluate the statistical significance of the variance. Values

of *$p < 0.05$, **$p < 0.01$, ***$p < 0.001$ ****$p < 0.0001$ were considered statistically significant.

3 Results and discussion

3.1 Morphology and structural characterization

As schematically illustrated in Scheme 1, the TiO$_2$ nanofilm on glass substrate was prepared by ALD. From the thermodynamic and kinetic point of view, the reaction of TiO$_2$ by TDMAT and H$_2$O can be separated into two half-reactions, which are described as follows [41, 42]:

$$Ti\big(N(CH_3)_2\big)_4 + TiO_2-OH* \rightarrow NH(CH_3)_2 \\ + TiO_2-O-Ti\big(N(CH_3)_2\big)_3* \quad (3)$$

$$TiO_2-O-Ti\big(N(CH_3)_2\big)_3* + 2H_2O \\ \rightarrow TiO_2-TiO_2-OH* + 3\big(NH(CH_3)_2\big) \quad (4)$$

where the asterisks denote the functional groups absorbed on the surface of the glass substrate. The growth mechanism of TiO$_2$ nanofilm can be explained in the following steps:

(1) The vapor pulse of the precursor TDMAT entered the reaction formula, then chemisorption reaction occurred on the exposed glass substrate surface.

(2) The cleaning gas N$_2$ brought the excess precursor TDMAT vapor which was not adsorbed by the substrate surface, and the reaction product methylamine (NH(CH$_3$)$_2$) out of the reaction chamber.

(3) Water vapor entered the reaction chamber and reacted with the TDMAT precursor adsorbed on the surface of glass substrate.

(4) The cleaning gas N$_2$ brought the excess water vapor and the by-product methylamine out of the reaction chamber.

The first stage was the chemisorption of TDMAT molecules by active sites of surface and the exchange of ligand. It usually happened easily even at very low operating temperatures, which was attributed to high reactivity of both TDMAT and OH groups. The subsequent step was the purge of remained TDMAT and reaction products (NH(CH$_3$)$_2$) from the reaction chamber. The next step was to introduce H$_2$O into the ALD chamber and perform the oxidation reaction. After the reaction process was completed, an atomically-layered TiO$_2$ film was formed on the surface in which all Ti atoms were connected to each other by O atoms. After several cycles of reaction, TiO$_2$ nanofilm was formed on the surface of glass substrate. Because the two half-reactions were carried out through a cycle, the film thickness could be adjusted with atomic-level accuracy and the film uniformity could be guaranteed. Subsequently, the silver nitrate solution was dropped onto the surface of the film. When TiO$_2$ nanofilm was irradiated with UV light, holes and electrons were generated as shown in Eq. (5), where hv is the energy absorbed:

$$TiO_2 \xrightarrow{hv} h^+ + e^- \quad (5)$$

There were silver ions (Ag$^+$) and nitrate ions (NO$_3^-$) in the AgNO$_3$ aqueous solution. The silver ions gained a generated electron and, consequently, silver metal was deposited onto the TiO$_2$ surface, as shown in Eq. (6):

$$AgNO_3 \xrightarrow{H_2O} Ag^+ + NO_3^- \xrightarrow{e^-} Ag(s) \quad (6)$$
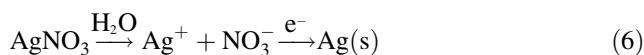
SEM images exhibited the morphology of the samples.
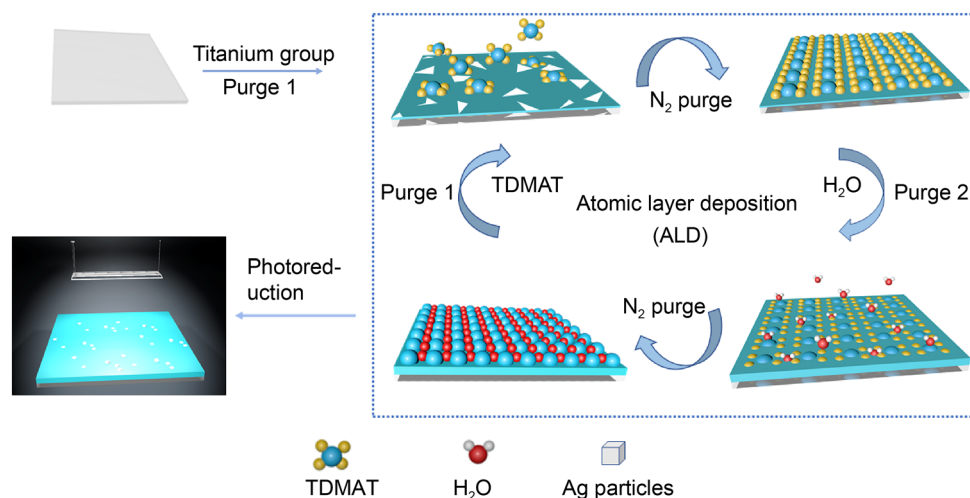
Scheme 1 Illustration of synthesis process of TiO$_2$/Ag coating
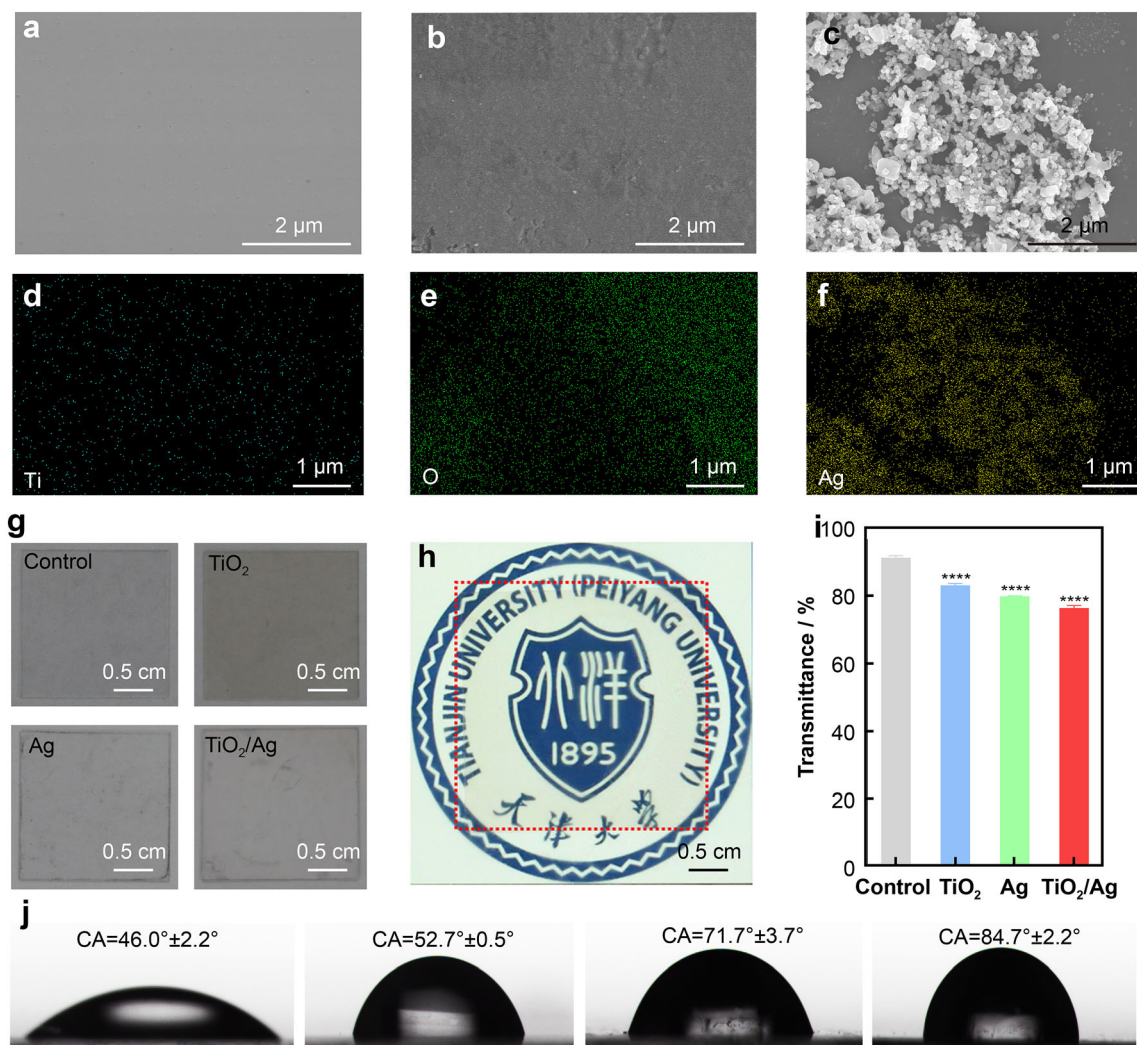
Fig. 1 Morphologies and characterization of synthesized materials: SEM images of **a** glass slide, **b** TiO$_2$ and **c** TiO$_2$/Ag; **d–f** SEM element mapping images of TiO$_2$/Ag; **g–i** light transmittance of TiO$_2$/Ag film; **j** water contact angles of glass, TiO$_2$, Ag and TiO$_2$/Ag, in which data represent mean $\pm$ standard deviation (n = 3 independent experiments per group). Significance was assessed using a one-way ANOVA with Dunnett's multiple comparisons (*$p < 0.05$, **$p < 0.01$, ***$p < 0.001$, ****$p < 0.0001$)

As shown in Fig. 1a, b, TiO$_2$ deposited by ALD formed a uniform and flat coating. Further, in Fig. 1c, the SEM image of TiO$_2$/Ag nanofilm exhibited that the size of photo-reduced silver nanoparticles was 200–800 nm, with slight agglomeration. The main reason for the agglomeration may due to the longer light irradiation. Elemental mappings further confirmed the successful deposition of silver nanoparticles on TiO$_2$ nanofilm (Fig. 1d–f).

Considering the subsequent antibacterial application of the coating on the touch screen, the transmittance of the sample was studied. The visible light transmittance of the TiO$_2$ nanofilm reached 83.2%. Even after adding photo-reduced silver particles, the light transmittance could still be maintained at about 76.4%, which satisfied the standard of the screen surface (Fig. 1g). The thickness of the

nanofilm was proportional to the number of ALD cycles, thus the transmittance of the samples can be controlled and adjusted (Fig. 1h, i). The hydrophilicity and hydrophobicity of the coating would affect its antibacterial effect, so water contact angle was also measured. The contact angles of glass slide, TiO$_2$ film, Ag film, and TiO$_2$/Ag film were 46.0°, 52.7°, 71.7°, and 84.7°, respectively (Fig. 1j). The result demonstrated the hydrophilicity of the samples, which were not conducive to the adhesion of bacteria.

The UV–Vis spectra (Fig. 2a) could reflect the optical property of TiO$_2$, Ag, and TiO$_2$/Ag nanofilms. Obviously, the optical absorbance of TiO$_2$ nanofilm mainly focused on the ultraviolet region, while Ag particles could absorb partial visible light. After Ag nanoparticles were deposited on TiO$_2$ nanofilm, the absorption edge of TiO$_2$/Ag had a red shift compared with separate TiO$_2$ or Ag. It may be
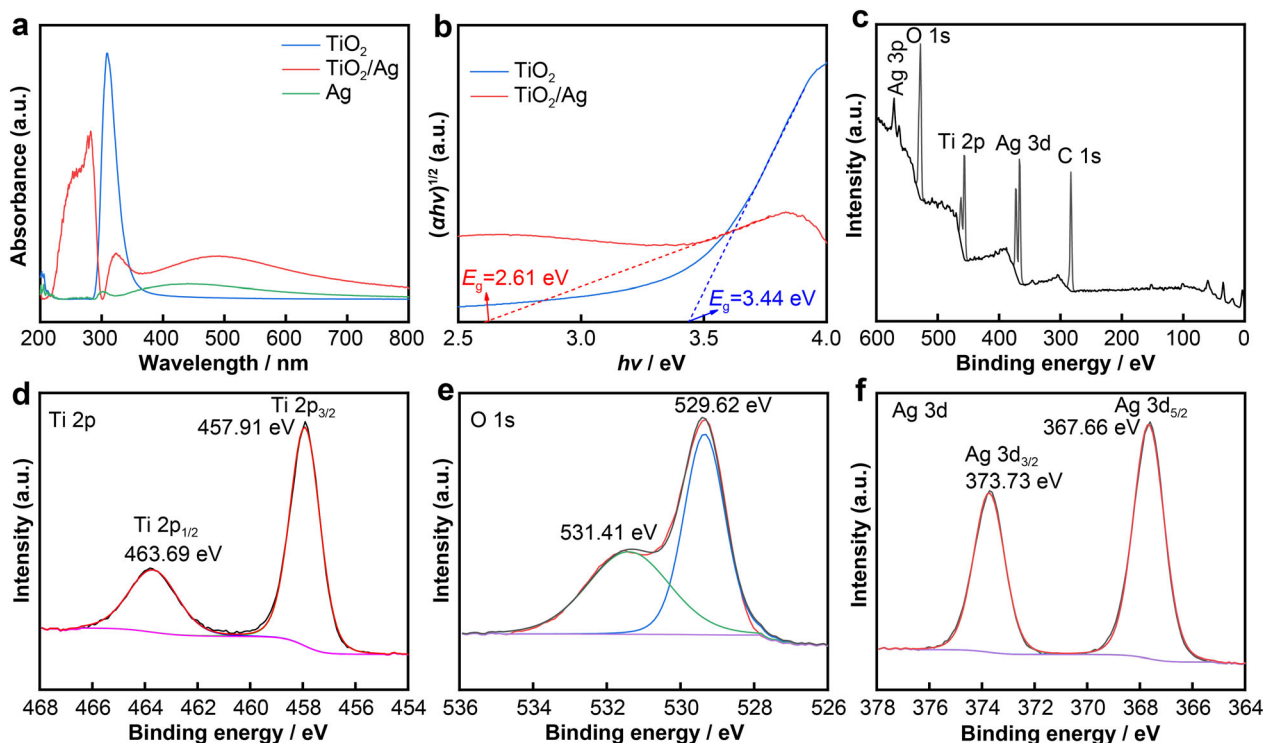
Fig. 2 Light absorption and XPS spectra of synthesized materials: **a** UV–Vis spectra (200–800 nm); **b** band gap of TiO₂ and TiO₂/Ag; **c** XPS spectrum of TiO₂/Ag; corresponding narrow scan of **d** Ti 2p, **e** O 1s, and **f** Ag 3d

based on the local plasmon resonance effect of Ag nanoparticles [43]. The red shift of the absorption curve led to a decrease in the band gap energy and recombination rate, thereby increasing the effect of photocatalytic activity.

The calculation of the semiconductor band gap was expressed by the following equation:

$$(\alpha h v)^n = C(h v - E_g) \tag{7}$$

where α is the absorption coefficient, hv is the absorption energy, C is a parameter associated with the valence and conduction band, and E_g is the band gap. The digit of n depends on the nature of the transition. In our case, for an indirect band gap, the value of n is 1/2. The variation of $(\alpha h v)^{1/2}$ with photon energy is shown in Fig. 2b. The band gaps were determined to be about 3.44 eV of TiO₂ and 2.61 eV of TiO₂/Ag, respectively, by extrapolation of the linear portion of the absorption coefficient α to zero for indirect-band-gap nanoparticles. When the band gap is reduced, the spectral absorption range of TiO₂ will be broadened, from only absorbing ultraviolet light originally to visible light. Besides, the yield of photogenerated electron–hole pair will also increase because of the shortening of band gap [44].

XPS measurements were conducted to verify the surface components and valence states of TiO₂/Ag nanofilm in Fig. 2c. The survey spectra of TiO₂/Ag nanofilm indicated the signal peaks corresponding to Ag, Ti, O and C

elements. The adventitious C 1s peak might lead to the contamination because the samples were exposed to air atmosphere. By fitting the high-resolution spectra, the binding energies centered at 457.91 and 463.69 eV corresponded to the 2p₃/₂ and 2p₁/₂ core levels of Ti⁴⁺ (Fig. 2d) [45, 46]. Figure 2e displays the O 1s spectra with peaks at 529.62 and 531.41 eV. The former was attributed to oxygen lattice, while the latter was correlated to surface hydroxyl groups [47]. 367.66 and 373.73 eV in the high resolution XPS (HRXPS) spectrum corresponded to Ag 3d₅/₂ and Ag 3d₃/₂, respectively; and the splitting of the 3d doublet was about 6 eV, indicating the silver was of metallic nature (Fig. 2f) [48].

3.2 Photocatalytic performance

Photocurrent response and EIS were utilized to characterize the photo-electrical properties of photocatalysts. It is widely accepted that the photocurrent intensity is decided by the separation efficiency of photogenerated carriers. As shown in Fig. 3a, the TiO₂ nanofilm had a weak current response under dark conditions but exhibited a stable current when exposed to xenon lamp irradiation. What's more, the composite film had a larger photocurrent response than the pure TiO₂ film. This indicated that the recombination of Ag particles could improve the separation of electron–hole pairs and transition efficiency of carriers. As shown in
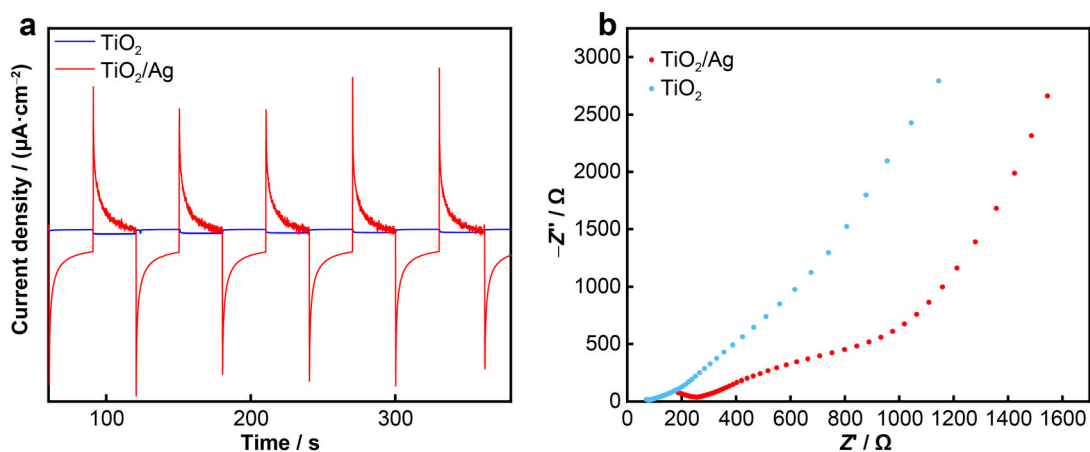
Fig. 3 Photoelectrochemical performance of samples: **a** photocurrent responses and **b** EIS plots of TiO_2 and TiO_2/Ag, where Z' is real part of impedance and Z'' is imaginary part of impedance

Fig. 3b, the diameter of Nyquist semicircle of TiO_2 was obviously shortened after the deposition of Ag particles, suggesting that the carriers transfer resistance was smaller.

Further, electron spin resonance (ESR) measurement was used to study generation process of ROS (Fig. 4). It can be seen that $\cdot OH$ and $\cdot O_2^-$ were detected under stimulated sunlight, while no signals for these two species were detected in the dark. In addition, it is indicated that the TiO_2/Ag heterojunction can provide more photogenerated holes and electrons than TiO_2 nanofilm to generate more ROS, which further supported the photocurrent and EIS test results. This was due to the localized plasmon resonance (LSPR) effect on the surface of Ag nanoparticles. After being excited under the irradiation of visible light, Ag nanoparticles can induce the transition of electron from the valence band (VB) of TiO_2 to the conduction band (CB), leaving holes in the VB. The photo-generated electrons reacted with O_2 adsorbed on the surface of TiO_2 to generate $\cdot O_2^-$, while the holes in the CB of TiO_2 have

more positive potential to oxidize OH^- and produce $\cdot OH$. Therefore, the TiO_2/Ag nanofilm can generate more ROS [49]. As the product of photocatalysis, ROS bears the important responsibility of killing bacteria, which is exactly the antibacterial mechanism of this study. This will be further elaborated in the following text.

3.3 In vitro antibacterial property

Two typical pathogenic bacteria, *S. aureus* and *E. coli* were chosen to evaluate the antibacterial performance of the coating. It can be seen from Fig. 5a–d that after 5 min of exposure to the simulated sunlight, the bacterial colonies of the TiO_2 group and the Ag group were slightly reduced compared to the control group. However, the doping of silver particles improved the photocatalytic activity. The bacterial colony reduction of the TiO_2/Ag group was the most significant, whose antibacterial efficiency against *S. aureus* and *E. coli* were 98.6% and 98.2%, respectively.
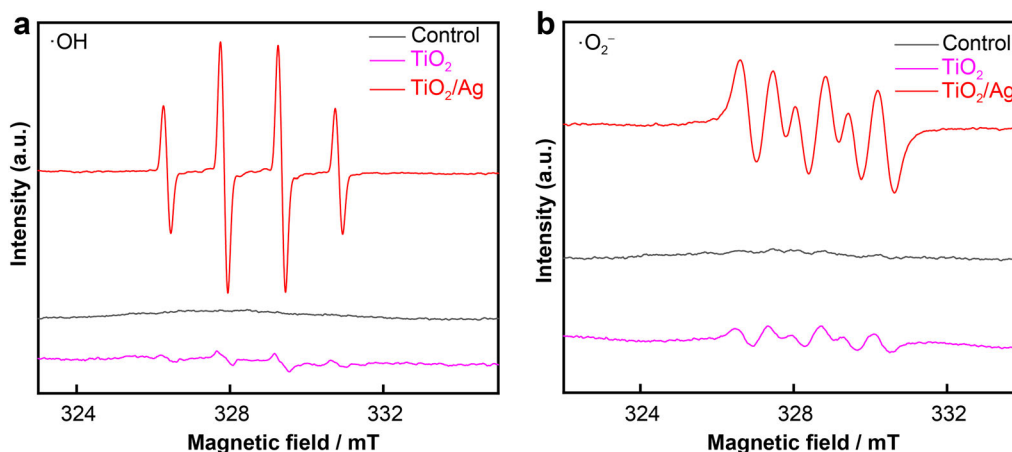

Fig. 4 ESR spectra of TiO_2 and TiO_2/Ag with and without light irradiation: **a** $\cdot OH$ and **b** $\cdot O_2^-$
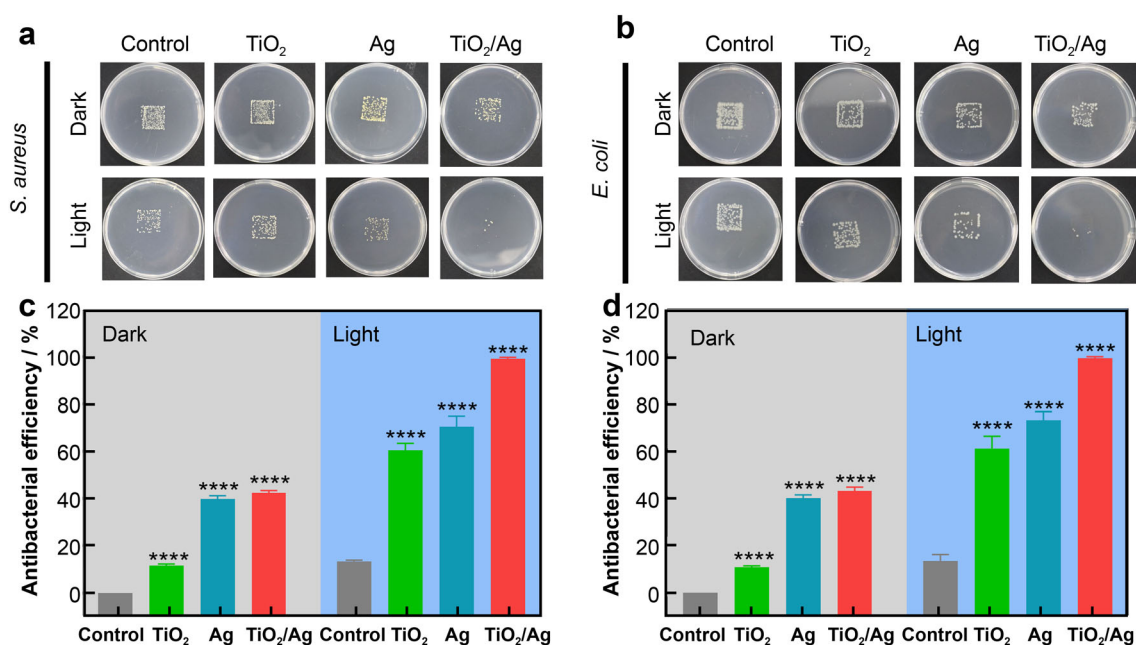
Fig. 5 Antibacterial activity of TiO₂, Ag and TiO₂/Ag: **a** spread plate of *S. aureus* and **c** corresponding antibacterial efficiency; spread plate of **b** *E. coli* and **d** corresponding antibacterial efficiency. Data represents mean ± standard deviation ($n = 3$ independent experiments per group; $*p < 0.05$, $**p < 0.01$, and $***p < 0.001$, $****p < 0.0001$)

The results of antibacterial activities also agreed with photocatalytic results. That is to say, better photocatalytic performance means more ROS generated during visible light irradiation, thus providing better antibacterial property [50].

The bacterial morphologies of representative samples of different groups under xenon lamp irradiation were examined by SEM. It can be seen from Fig. 6 that the bacteria in the control group were smooth, complete, and representative. In contrast, the bacterial membranes of the TiO₂ group and the Ag group showed slight wrinkles and ruptures. However, the bacterial membrane of the TiO₂/Ag group

exhibited obvious deformation and cracking, whether it was *S. aureus* or *E. coli*. It has been verified that ROS could react with membranes through multiple mechanisms, causing them to rupture, inducing protein leakage, and even entering bacteria to damage DNA and organelles [51]. In addition to the effect of ROS, the release of Ag⁺ also played a certain role in the damage of the bacterial membrane. The release of Ag⁺ which interacted with the thiol group of a bacterial enzyme interrupted the respiratory mechanism by having a lethal effect on the bacteria [52].

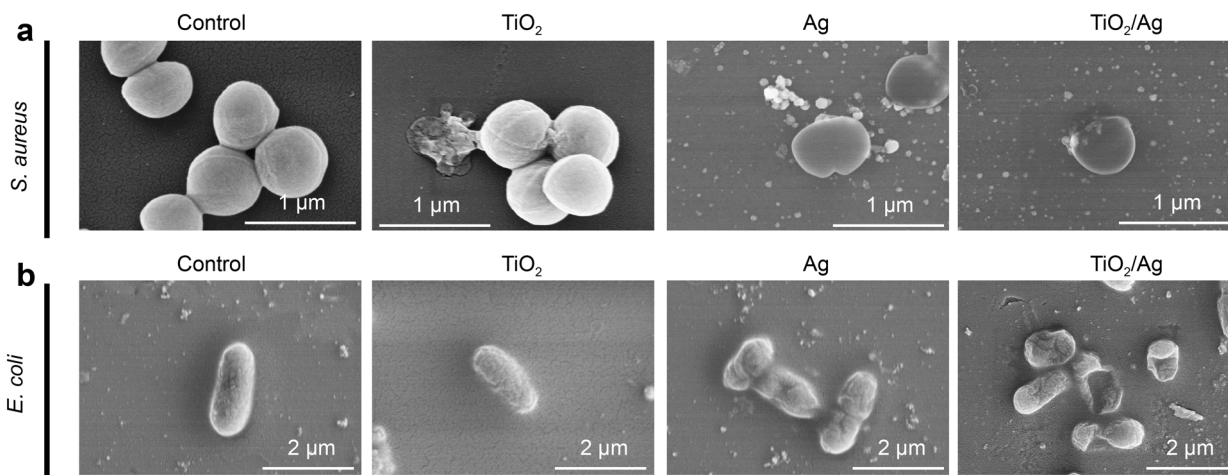The mechanism of the photocatalytic disinfection was schematically illustrated in Fig. 7. As one of traditional

Fig. 6 SEM images of bacteria with TiO₂, Ag, and TiO₂/Ag under 5 min stimulated solar irradiation: **a** *S. aureus* and **b** *E. coli*
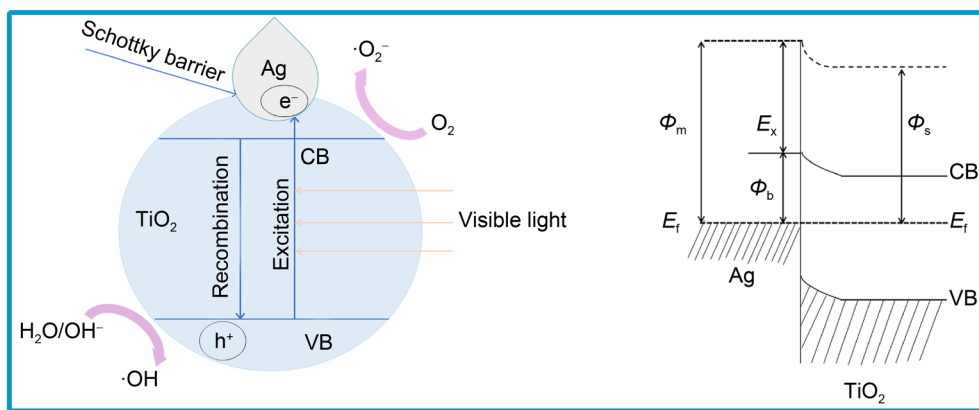
Fig. 7 Schematic illustration of mechanism of enhanced photocatalysis of TiO$_2$/Ag, where Φ_m is work function of metal, Φ_s is work function of semiconductor, Φ_b is Schottky barrier, E_x is electron affinity, E_f is Fermi level

n-type semiconductors, when TiO$_2$ was irradiated by stimulated sunlight, the electrons in its VB would be excited to the CB. These electrons would be removed by O$_2$, so that ·O$_2^-$ was produced. At the same time, the holes on the VB trapped the H$_2$O on the surface to oxidize them to ·OH. However, when Ag particles were deposited on the surface of TiO$_2$ and in contact with each other, since the Fermi level of TiO$_2$ was higher than Ag, electrons will transfer from TiO$_2$ to Ag until the Fermi levels of them were equal. Therefore, in the space charge layer formed after the electrical contact, the surface of Ag got excessive quantity of negative charges, while the TiO$_2$ surface left excessive quantity of holes, which formed a Schottky heterojunction at the interface of TiO$_2$ and Ag. The Ag particles acted as electron traps to leave electrons and holes in two different phases, inhibiting the recombination of electron–hole pairs, thereby improving the efficiency of photocatalysis.

3.4 Cytotoxicity evaluation

The MTT assay was used to examine the effects of different samples on the growth of L929 cells. Since the film was used in vitro, the cells were only cultured for one day. It can be seen from Fig. 8 that the effect of light on cell viability was almost negligible. The cell survival rate of the TiO$_2$ group was about 90%, while the cell viability of final group could still be maintained at about 85%, indicating that the material will not have a health impact on the human body when applied in vitro.

4 Conclusion

In this work, TiO$_2$ nanofilm was prepared by atomic layer deposition, and then Ag particles were deposited on the film by photo-reduction to prepare photocatalytic TiO$_2$/Ag
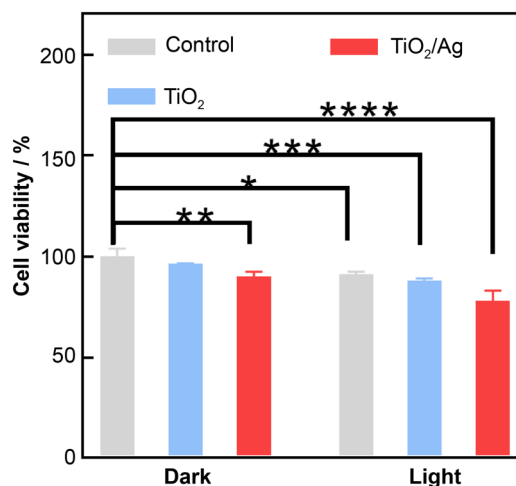

Fig. 8 L929 assay of cell viabilities with different samples after co-cultured for 24 h. Data are presented as mean ± standard deviations from a representative experiment. Error bar represents standard deviation ($n = 3$ independent experiments per group, *$p < 0.05$, **$p < 0.01$, ***$p < 0.001$, ****$p < 0.0001$)

coating. Because the Schottky heterojunction was formed at the interface between TiO$_2$ and Ag, the electron–hole recombination rate of TiO$_2$/Ag was suppressed. Besides, the photocatalytic efficiency of TiO$_2$/Ag was greatly increased by generating more ROS. Its visible light catalytic antibacterial effect was better than that of untreated TiO$_2$ nanofilm. The antibacterial efficiency against *S. aureus* and *E. coli* in vitro under the irradiation of stimulated sunlight reached 98.2% and 98.6%, respectively. Meanwhile, the deposited film had great light transmittance and biocompatibility with/without light irradiation, with a good prospect not only for the traditional antibacterial mode but also in the field of surface antibacterial application.

Declarations

Conflict of interests The authors declare that they have no conflict of interest.

References

[1] Deng W, Sun YJ, Yao XX, Subramanian K, Ling C, Wang HB, Chopra SS, Xu BB, Wang JX, Chen JF, Wang D, Amancio H, Pramana S, Ye RQ, Wang S. Masks for COVID-19. Adv Sci. 2021. https://doi.org/10.1002/advs.202102189.

[2] Hosseini M, Chin AWH, Williams MD, Behzadinasab S, Falkinham JO, Poon LLM, Ducker WA. Transparent anti-SARS-CoV-2 and antibacterial silver oxide coatings. Acs Appl Mater Interfaces. 2022. https://doi.org/10.1021/acsami.1c20872.

[3] Wang X, Wang Y, Bi S, Wang YG, Chen XG, Qiu LY, Sun JQ. Optically transparent antibacterial films capable of healing multiple scratches. Adv Funct Mater. 2014;24(3):403. https://doi.org/10.1002/adfm.201302109.

[4] Yu P, Han YJ, Han DL, Liu XM, Liang YQ, Li ZY, Zhu SL, Wu SL. In-situ sulfuration of Cu-based metal-organic framework for rapid near-infrared light sterilization. J Hazard Mater. 2020;390: 122126. https://doi.org/10.1016/j.jhazmat.2020.122126.

[5] Zeng X, Mccarthy DT, Deletic A, Zhang X. Silver/reduced graphene oxide hydrogel as novel bactericidal filter for point-of-use water disinfection. Adv Funct Mater. 2015;25(27):4344. https://doi.org/10.1002/adfm.201501454.

[6] Li P, Wu HX, Dong A. Ag/AgX nanostructures serving as antibacterial agents: achievements and challenges. Rare Met. 2022;41(2):519. https://doi.org/10.1007/s12598-021-01822-0.

[7] Liu W, Ou-Yang W, Zhang C, Wang QS, Pan XB, Huang PS, Zhang CN, Li YJ, Kong DL, Wang WW. Synthetic polymeric antibacterial hydrogel for methicillin-resistant *Staphylococcus aureus*-infected wound healing: nanoantimicrobial self-assembly, drug- and cytokine-free strategy. ACS Nano. 2020;14(10): 12905. https://doi.org/10.1021/acsnano.0c03855.

[8] Hamad M, Al-Marzooq F, Orive G, Al-Tel TH. Superbugs but no drugs: steps in averting a post-antibiotic era. Drug Discov Today. 2019;24(12):2225. https://doi.org/10.1016/j.drudis.2019.08.004.

[9] Hwang GB, Huang H, Wu G, Shin J, Kafizas A, Karu K, Toit HD, Alotaibi AM, Mohammad-Hadi L, Allan E, Macrobert AJ, Gavriilidis A, Parkin IP. Photobactericidal activity activated by thiolated gold nanoclusters at low flux levels of white light. Nat Commun. 2020;11(1):1207. https://doi.org/10.1038/s41467-020-15004-6.

[10] Natan M, Gutman O, Lavi R, Margel S, Banin E. Killing mechanism of stable N-halamine cross-linked polymethacrylamide nanoparticles that selectively target bacteria. ACS Nano. 2015;9(2):1175. https://doi.org/10.1021/nn507168x.

[11] Ren Y, Liu HP, Liu XM, Zheng YF, Li ZY, Li CY, Yeung KWK, Zhu SL, Liang YQ, Cui ZD, Wu SL. Photoresponsive materials for antibacterial applications. Cell Rep Phys Sci. 2020; 1(11): 100245. https://doi.org/10.1016/j.xcrp.2020.100245.

[12] Luo Y, Liu XM, Tan L, Li ZY, Yeung KWK, Zheng YF, Cui ZD, Liang YQ, Zhu SL, Li CY, Wang XB, Wu SL. Enhanced photocatalytic and photothermal properties of ecofriendly metal-organic framework heterojunction for rapid sterilization. Chem Eng J. 2021;405:126730. https://doi.org/10.1016/j.cej.2020.126730.

[13] Li J, Li ZY, Liu XM, Li CY, Zheng YF, Yeung KWK, Cui ZD, Liang YQ, Zhu SL, Hu WB, Qi YJ, Zhang TJ, Wang XB, Wu SL. Interfacial engineering of Bi₂S₃/Ti₃C₂Tₓ MXene based on work function for rapid photo-excited bacteria-killing. Nat Commun. 2021;12(1):1224. https://doi.org/10.1038/s41467-021-21435-6.

[14] Han D, Li Y, Liu XM, Yeung KWK, Zheng YF, Cui ZD, Liang YQ, Li ZY, Zhu SL, Wang XB, Wu SL. Photothermy-strengthened photocatalytic activity of polydopamine-modified metal-organic frameworks for rapid therapy of bacteria-infected wounds. J Mater Sci Technol. 2021;62:83. https://doi.org/10.1016/j.jmst.2020.05.055.

[15] Han D, Li Y, Liu XM, Li B, Han Y, Zheng YF, Yeung KWK, Li CY, Cui ZD, Liang YQ, Li ZY, Zhu SL, Wang XB, Wu SL. Rapid bacteria trapping and killing of metal-organic frameworks strengthened photo-responsive hydrogel for rapid tissue repair of bacterial infected wounds. Chem Eng J. 2020;396:125194. https://doi.org/10.1016/j.cej.2020.125194.

[16] Chai M, An MW, Zhang XU, Chu P. In vitro and in vivo antibacterial activity of graphene oxide-modified porous TiO₂ coatings under 808-nm light irradiation. Rare Met. 2022;41(2): 540. https://doi.org/10.1007/s12598-021-01754-9.

[17] Yang B, Chen Y, Shi JL. Reactive oxygen species (ROS)-based nanomedicine. Chem Rev. 2019;119(8):4881. https://doi.org/10.1021/acs.chemrev.8b00626.

[18] D'Autréaux B, Toledano MB. ROS as signalling molecules: mechanisms that generate specificity in ROS homeostasis. Nat Rev Mol Cell Biol. 2007;8(10):813. https://doi.org/10.1038/nrm2256.

[19] Lv R, Liang YQ, Li ZY, Zhu SL, Cui ZD, Wu SL. Flower-like CuS/graphene oxide with photothermal and enhanced photocatalytic effect for rapid bacteria-killing using visible light. Rare Met. 2022;41(2):639. https://doi.org/10.1007/s12598-021-01759-4.

[20] Han D, Yu PL, Liu XM, Xu YD, Wu SL. Polydopamine modified CuS@HKUST for rapid sterilization through enhanced photothermal property and photocatalytic ability. Rare Met. 2022;41(2):663. https://doi.org/10.1007/s12598-021-01786-1.

[21] Kanagamani K, Muthukrishnan P, Saravanakumar K, Shankar K, Kathiresan A. Photocatalytic degradation of environmental perilous gentian violet dye using leucaena-mediated zinc oxide nanoparticle and its anticancer activity. Rare Met. 2019;38(4): 277. https://doi.org/10.1007/s12598-018-1189-5.

[22] Han Z, Liu XM, Tan L, Li ZY, Zheng YF, Yeung KWY, Cui ZD, Liang YQ, Zhu SL, Wu SL. Photothermal-controlled sustainable degradation of protective coating modified Mg alloy using near-infrared light. Rare Met. 2021;40(9):2538. https://doi.org/10.1007/s12598-020-01667-z.

[23] Yang H, Zhai LS, Li K, Liu X, Deng B, Xu WL. A highly efficient nano-graphite-doped TiO₂ photocatalyst with a unique sea-island structure for visible-light degradation. Catal Sci Technol. 2020;1(4):1117. https://doi.org/10.1039/c9cy02179e.

[24] Deng H, Wang XC, Wang L, Li ZJ, Liang PL, Ou JA, Liu K, Yuan LY, Jiang ZY, Zheng LR, Chai ZF, Shi WQ. Enhanced photocatalytic reduction of aqueous Re (VII) in ambient air by amorphous TiO₂/g-C₃N₄ photocatalysts: implications for Tc (VII) elimination. Chem Eng J. 2020;401:125977. https://doi.org/10.1016/j.cej.2020.125977.

[25] Moridi Mahdieh Z, Shekarriz S, Afshar Taromi F, Montazer M. A new method for in situ synthesis of Ag-TiO₂ nanocomposite particles on polyester/cellulose fabric by photoreduction and self-cleaning properties. Cellulose. 2018;25(4):2355. https://doi.org/10.1007/s10570-018-1694-6.

[26] Ren Y, Han YJ, Li ZY, Liu XM, Zhu SL, Liang YQ, Yeung KWK, Wu SL. Ce and Er co-doped TiO₂ for rapid bacteria-killing using visible light. Bioact Mater. 2020;5(2):201. https://doi.org/10.1016/j.bioactmat.2020.02.005.

[27] Yin L, Fu ZX, Li Y, Liu B, Lin ZJ, Lu JY, Chen X, Han XP, Deng YD, Hu WB, Zou DR, Zhong C. Enhanced antibacterial properties of biocompatible titaniumvia electrochemically deposited Ag/TiO₂ nanotubes and chitosan–gelatin–Ag–ZnO complex coating. RSC Adv. 2019;9(8):4521. https://doi.org/10.1039/C8RA07682K.

[28] Wang R, Shi MS, Xu FY, Qiu Y, Zhang P, Shen KL, Zhao Q, Yu JG, Zhang YF. Graphdiyne-modified TiO₂ nanofibers with osteoinductive and enhanced photocatalytic antibacterial activities to prevent implant infection. Nat Commun. 2020;11(1):4465. https://doi.org/10.1038/s41467-020-18267-1.

[29] Chen SF, Li JP, Qian K, Xu WP, Lu Y, Huang WX, Yu SH. Large scale photochemical synthesis of M@TiO₂ nanocomposites (M = Ag, Pd, Au, Pt) and their optical properties, CO oxidation performance, and antibacterial effect. Nano Res. 2010;3(4):244. https://doi.org/10.1007/s12274-010-1027-z.

[30] Shim J, Seo Y, Oh B, Cho M. Microbial inactivation kinetics and mechanisms of carbon-doped TiO₂ (C-TiO₂) under visible light. J Hazard Mater. 2016;306:133. https://doi.org/10.1016/j.jhazmat.2015.12.013.

[31] Li J, Song S, Meng JS, Tan L, Liu XM, Zheng YF, Li ZY, Yeung KWK, Cui ZD, Liang YQ, Zhu SL, Zhang XC, Wu SL. 2D MOF periodontitis photodynamic ion therapy. J Am Chem Soc. 2021;143(37):15427. https://doi.org/10.1021/jacs.1c07875.

[32] Zhao J, Nunn WT, Lemaire PC, Lin Y, Dickey MD, Oldham CJ, Walls HJ, Peterson GW, Losego MD, Parsons GN. Facile conversion of hydroxy double salts to metal-organic frameworks using metal oxide particles and atomic layer deposition thin-film templates. J Am Chem Soc. 2015;137(43):13756. https://doi.org/10.1021/jacs.5b08752.

[33] Huang L, Su K, Zheng YF, Yeung KWK, Liu XM. Construction of TiO₂/silane nanofilm on AZ31 magnesium alloy for controlled degradability and enhanced biocompatibility. Rare Met. 2019;38(6):588. https://doi.org/10.1007/s12598-018-1187-7.

[34] Li Y, He J, Ye HX, Zhao CC, Zhu WW, Lu X, Ren FZ. Atomic layer deposition of zinc oxide onto 3D porous iron scaffolds for bone repair: in vitro degradation, antibacterial activity and cytocompatibility evaluation. Rare Met. 2022;41(2):546. https://doi.org/10.1007/s12598-021-01852-8.

[35] Díaz-Uribe C, Viloria J, Cervantes L, Vallejo W, Navarro K, Romero E, Quiñones C. Photocatalytic activity of Ag-TiO₂ composites deposited by photoreduction under UV irradiation. Int J Photoenergy. 2018;2018:1. https://doi.org/10.1155/2018/6080432.

[36] Kotesh Kumar M, Bhavani K, Nareshb G, Srinivas B, Venugopal A. Plasmonic resonance nature of Ag-Cu/TiO₂ photocatalyst under solar and artificial light: synthesis, characterization and evaluation of H₂O splitting activity. Appl Catal B. 2016;199:282. https://doi.org/10.1016/j.apcatb.2016.06.050.

[37] Yang K, Lu Y, Hsu Y, Lin C, Tseng C, Liou SYH, Kumar K, Wei DH, Dong CL, Chen CL. Plasmon-induced visible-light photocatalytic activity of Au nanoparticle-decorated hollow mesoporous TiO2: a view by X-ray spectroscopy. J Phys Chem C. 2018;122(12):6955. https://doi.org/10.1021/acs.jpcc.8b00205.

[38] Kiran Gupta RPSA. Photocatalytic antibacterial performance of TiO2 and Ag-doped TiO2 against S. Aureus. P. Aeruginosa and E. Coli. Beilstein J Nanotechnol. 2013;4:345. https://doi.org/10.3762/bjnano.4.40.

[39] Jia Z, Xiu P, Li M, Xu XC, Shi YY, Cheng Y, Wei SC, Zheng YF, Xi TF, Cai H, Liu ZJ. Bioinspired anchoring AgNPs onto micro-nanoporous TiO₂ orthopedic coatings: trap-killing of bacteria, surface-regulated osteoblast functions and host responses. Biomaterials. 2016;75:203. https://doi.org/10.1016/j.biomaterials.2015.10.035.

[40] Nel A, Xia T, Mädler L, Li N. Toxic potential of materials at the nanolevel. Science. 2006;311(5761):622. https://doi.org/10.1126/science.1114397.

[41] Xie Q, Jiang YL, Detavernier C, Deduytsche D, Van Meirhaeghe RL, Ru GP, Li BZ, Qu XP. Atomic layer deposition of TiO₂ from tetrakis-dimethyl-amido titanium or Ti isopropoxide precursors and H₂O. J Appl Phys. 2007;102(8):83521. https://doi.org/10.1063/1.2798384.

[42] Zhuiykov S, Akbari MK, Hai ZY, Xue CY, Xu HY, Hyde L. Wafer-scale fabrication of conformal atomic-layered TiO₂ by atomic layer deposition using tetrakis (dimethylamino) titanium and H₂O precursors. Mater Des. 2017;120:99. https://doi.org/10.1016/j.matdes.2017.02.016.

[43] Cozzoli PD, Comparelli R, Fanizza E, Curri ML, Agostiano A, Laub D. Photocatalytic synthesis of silver nanoparticles stabilized by TiO₂ nanorods: a semiconductor/metal nanocomposite in homogeneous nonpolar solution. J Am Chem Soc. 2004;126(12):3868. https://doi.org/10.1021/ja0395846.

[44] Rengaraj S, Li XZ. Enhanced photocatalytic activity of TiO₂ by doping with Ag for degradation of 2,4,6-trichlorophenol in aqueous suspension. J Mol Catal A Chem. 2006;243(1):60. https://doi.org/10.1016/j.molcata.2005.08.010.

[45] Stathatos E, Lianos P, Falaras P, Siokou A. Photocatalytically deposited silver nanoparticles on mesoporous TiO₂ films. Langmuir. 2000;16(5):2398. https://doi.org/10.1021/la981783t.

[46] Dong S, Dong SS, Zhou DD, Zhou X, Ma DM, Du YL. Synthesis of Er³⁺: Al₂O₃-doped and rutile-dominant TiO₂ composite with increased responsive wavelength range and enhanced photocatalytic performance under visible light irradiation. J Mol Catal A Chem. 2015;407:38. https://doi.org/10.1016/j.molcata.2015.06.016.

[47] Yu J, Xiong JF, Cheng B, Liu SW. Fabrication and characterization of Ag-TiO₂ multiphase nanocomposite thin films with enhanced photocatalytic activity. Appl Catal B. 2005;60(3):211. https://doi.org/10.1016/j.apcatb.2005.03.009.

[48] Wang X, Su K, Tan L, Liu XM, Cui ZD, Jing DD, Yang XJ, Liang YQ, Li ZY, Zhu SL, Yeung KWK, Zheng D, Wu SL. Rapid and highly effective noninvasive disinfection by hybrid Ag/CS@MnO₂ nanosheets using near-infrared light. ACS Appl Mater Interfaces. 2019;11(16):15014. https://doi.org/10.1021/acsami.8b22136.

[49] Tong ZW, Yang D, Sun YY, Jiang ZY. Biomimetic synthesis of C₃N₄/TiO₂/Ag nanosheet composites with high visible-light photocatalytic performance. RSC Adv. 2015;5(70):56913. https://doi.org/10.1039/C5RA06980G.

[50] Zhang Y, Liu XM, Li ZY, Zhu SL, Yuan XB, Cui ZD, Yang XJ, Chu PK, Wu SL. Nano Ag/ZnO-incorporated hydroxyapatite composite coatings: highly effective infection prevention and excellent osteointegration. ACS Appl Mater Interfaces. 2018;10(1):1266. https://doi.org/10.1021/acsami.7b17351.

[51] Liu H, Li JF, Liu XM, Li ZY, Zhang Y, Liang YQ, Zheng YF, Zhu SL, Cui ZD, Wu SL. Photo-sono interfacial engineering exciting the intrinsic property of herbal nanomedicine for rapid broad-spectrum bacteria killing. ACS Nano. 2021;15(11):18505. https://doi.org/10.1021/acsnano.1c08409.

[52] Xiu Z, Zhang QB, Puppala HL, Colvin VL, Alvarez PJJ. Negligible particle-specific antibacterial activity of silver nanoparticles. Nano Lett. 2012;12(8):4271. https://doi.org/10.1021/nl301934w.